applied system innovation

MDPI

Article

Examining Hybrid Nanofluid Flow Dynamics in the Conical Gap between a Rotating Disk and Cone Surface: An Artificial Neural Network Approach

Julien Moussa H. Barakat *, Zaher Al Barakeh and Raymond Ghandour

College of Engineering and Technology, American University of the Middle East, Egaila 54200, Kuwait; zaher.al-barakeh@aum.edu.kw (Z.A.B.); raymond.ghandour@aum.edu.kw (R.G.)
* Correspondence: julien.barakat@aum.edu.kw

Abstract: To comprehend the thermal regulation within the conical gap between a disk and a cone (TRHNF-DC) for hybrid nanofluid flow, this research introduces a novel application of computationally intelligent heuristics utilizing backpropagated Levenberg–Marquardt neural networks (LM-NNs). A unique hybrid nanoliquid comprising aluminum oxide, Al_2O_3, nanoparticles and copper, Cu, nanoparticles is specifically addressed. Through the application of similarity transformations, the mathematical model formulated in terms of partial differential equations (PDEs) is converted into ordinary differential equations (ODEs). The BVP4C method is employed to generate a dataset encompassing various TRHNF-DC scenarios by varying magnetic parameters and nanoparticles. Subsequently, the intelligent LM-NN solver is trained, tested, and validated to ascertain the TRHNF-DC solution under diverse conditions. The accuracy of the LM-NN approach in solving the TRHNF-DC model is verified through different analyses, demonstrating a high level of accuracy, with discrepancies ranging from 10^{-10} to 10^{-8} when compared with standard solutions. The efficacy of the framework is further underscored by the close agreement of recommended outcomes with reference solutions, thereby validating its integrity.

Keywords: hybrid nanofluid; flow dynamics; rotating disk; Levenberg–Marquardt; artificial neural network; accuracy assessment

Citation: Barakat, J.M.H.; Al Barakeh, Z.; Ghandour, R. Examining Hybrid Nanofluid Flow Dynamics in the Conical Gap between a Rotating Disk and Cone Surface: An Artificial Neural Network Approach. *Appl. Syst. Innov.* **2024**, *7*, 63. https://doi.org/10.3390/asi7040063

Academic Editor: Sergio Nardini

Received: 3 June 2024
Revised: 10 July 2024
Accepted: 17 July 2024
Published: 22 July 2024

1. Introduction

With the swift progress of nanoscience and contemporary scientific domains, nanostructured materials have emerged as a focal point for researchers. Nanofluids, characterized by the stable dispersion of small particles in the nanometer scale within base fluids, have emerged. Metal oxides and carbon materials are commonly employed in their creation, finding applications in thermal engineering, electronic devices, and fiber technology. The exploration of mass and heat transfer in nanoliquid motion along a rotating disk has garnered significant attention due to its diverse uses in electronic appliances and heat exchangers [1].

1.1. Cone–Disk Apparatus

Cone–disk apparatus exhibits versatility in its applications across various domains. For instance, this apparatus is instrumental in investigating the characteristics and stability of a particular fluid flow, identified as Oldroyd-B fluid, under specific circumstances [2]. Another application involves employing cone–disk devices for medical uses, as highlighted in the study by Spruell [3]. These cone–disk tools are integrated into gas turbine cooling systems, particularly within a conical diffuser [4]. In the realm of gas turbine systems, these instruments are utilized to improve cooling efficiency, potentially by refining air compression. The configuration appears pivotal in this endeavor. Choi [5] leads in the

utilization of nanoparticles comprising metals, oxides, and carbides dispersed in base fluids to enhance the heat conductivity of these fluids.

1.2. Research Methodologies

Investigations on the dynamics of nanofluid flow in cone–disk apparatus have attracted considerable interest from researchers.Turkilmazoglu [6] utilized a semi-analytical approach (HAM) to examine streamline motion along a spinning cone, producing thoroughly documented and successful results. Following stability analyses of the boundary layer, Garrett [7] delved into the inherent or convective nature of instability induced by the rotating cone. Furthermore, Towers et al. [8] scrutinized similarity solutions for compressible laminar flows subject to surface mass flux over an array of rotating cones.

Rasool and Zhang [9] investigated the influence of Darcy–Forchheimer viscoelastic nanofluid flow constrained by a nonlinear stretching surface, integrating Cattaneo–Christov heat–mass flux. Shirejini [10] utilized nanofluids to enhance heat transfer rates through a spinning method. The heat transfer characteristics of an electrically conducting fluid over a rotating infinite disk were examined by Turkyilmazoglu et al. [11], with applications spanning computer devices, thermal energy systems, rotating machinery, geothermal industry, electronic instruments, chemical processes, gas turbines, and medical apparatus. Kumar [12] employed the finite element method to analyze entropy generation in the radiative flow of a nanoliquid comprising aluminum oxide and copper nanoparticles between two coaxially rotating disks. Bhattacharyya [13] modeled heat flux in the flow of a nanoliquid containing carbon nanotubes between two coaxially stretchable rotating disks. A numerical study by Nazari et al. [14] simulated the non-Newtonian water/Al_2O_3 nanoliquid flow with nano-sized particles within a 2D square cavity featuring hot and cold lid-driven motion. Ahmed [15] scrutinized Maxwell fluid flow with the effects of homogeneous–heterogeneous reactions between heat conduction and two revolving disks. Additionally, Rashidi [16] conducted a numerical study to examine fluidic and thermal responses in variously configured containers filled with an Al_2O_3/water nanofluid and featuring a rectangular heated obstruction.

1.3. Magnetohydrodynamics

The core principle of Magnetohydrodynamics (MHD) revolves around controlling fluid flow. To achieve heightened thermal conductivity and enhanced heat transfer rates for effective cooling, one must consider the phenomenon of magnetic forces. Magnetic effects find applications in various medical treatments such as treating malignant tumors, managing blood pressure, alleviating arthritis, and therapeutic interventions for the brain. Siddiqui [17] explored the application of MHD fluid flow motion in the respiratory tract for disease monitoring. The Keller-box technique was utilized in [18] to numerically solve a problem involving swirling MHD fluid motion across a permeable surface. Oyelakin [19] investigated the influence of velocity slip in tangent hyperbolic nanoliquid flow and its heat transfer characteristics. Tlili [20] analyzed the magnetic flow of hybrid nanoliquid over a stretched surface with slip effects.

1.4. Hybrid Nanoliquids

In the contemporary realm of science and technology, hybrid nanoliquids have attracted significant attention from researchers due to their remarkable and potentially superior thermal characteristics, surpassing those of simple nanoliquids in enhancing heat transmission rates. Experimental studies have concluded that varying volume fractions of nano materials (ranging from 5 to 55%, with particle sizes of 1–100 nm) contribute to increased thermal conductance and improved heat transfer rates of base fluids [21]. An empirical investigation by [22] examined the impact of particle concentration and temperature on the viscous characteristics of minute particles of ZnO-MWCNTs/engine oil hybrid nanolubricant. The hydrodynamic stability of monophasic nanofluids based on the linear stability concept was underscored by [23].

1.5. Artificial Neural Networks

Artificial neural networks (ANNs) represent a crucial approach in artificial intelligence. ANNs exhibit evolutionary adaptability in numerous scenarios, leveraging information propagation over the network during learning, whether internally or externally. Throughout the learning process, ANNs generate a set of connections (weights) that effectively represent the training set. To tackle various problems based on differential equations, ANNs are extensively used, with problematic numerical outcomes often addressed by modeling ANNs and optimizing them through a combination of nonlinear and linear search algorithms. Recent advancements in stochastic numeric computer solvers have led to the development of nonlinear models for various domains. These include corneal aspects [24], astrophysical systems [25,26], delay differential equation-based mathematical models [27], financial models [28], dust density models [29], plasma physics [30], nonlinear Emden–Fowler equations [31], singular differential models [32], bioinformatics [33], atomic physics [34], fluid dynamics issues [35,36], electromagnetic phenomena [37], heat conduction [38], and ground motion prediction models [39]. These developments serve as strong motivation for researchers to explore stochastic methods and employ them in developing alternative, factual, and practical computer models for addressing fluid dynamics issues such as TRHNF-DC. Artificial neural networks (ANNs) improve the predictive accuracy of hybrid nanofluid flow dynamics in complex geometries, such as the conical gap between a rotating disk and cone surface, by effectively capturing nonlinear relationships. ANNs leverage large datasets to identify intricate patterns and insights in the flow dynamics, providing a deeper understanding of how different factors influence the system's behavior. Using ANNs enables optimization of parameters and conditions in the flow dynamics study, leading to more efficient and effective designs for applications involving hybrid nanofluids. Once trained, ANNs can quickly predict outcomes for new scenarios, significantly reducing the computational time and resources needed compared with traditional numerical simulation methods. ANNs are highly adaptable to various types of input data and scalable to larger and more complex problems, making them suitable for a wide range of applications in fluid dynamics research.

1.6. Objectives of the Study

The ongoing inquiry centers on the heat transfer facilitated by a hybrid nanoliquid coursing through the aperture between a cone and a disk. The disk and cone can rotate either parallel to each other, rotate in opposite directions with angular velocity, or maintain one in a stationary position relative to the other. Indeed, the literature indicates a gap in research concerning the examination of a three-dimensional hybrid nanoliquid flow involving a cone and disk configuration, whether in motion or stationary, and under the influence of a magnetic field. This study aims to address this gap by specifically investigating how copper (Cu) and aluminum dioxide (Al_2O_3) nanoparticles impact the thermophysical properties of water, offering valuable insights for various scientific and technological applications. Additionally, a secondary objective is to build upon the concepts outlined in [40,41], which are closely related to the current model and provide a foundation for further exploration. The primary aim of this study is to develop a mathematical framework for analyzing a rotating cone and disk system, considering both motion and stationary states, and exploring both counter-rotating and co-rotating scenarios. The governing flow equations are simplified into an ordinary system and solved using the BVP4C method. The uniqueness of this study lies in its original contributions to the field, addressing previously unexplored aspects of hybrid nanoliquid flow dynamics involving rotating cone and disk configurations. The study accomplishes similar objectives to the study made in [42], but relying on a different modeling approach.

The size of copper (Cu) and aluminum oxide (Al_2O_3) nanoparticles significantly impacts the thermal conductivity of the hybrid nanofluid, with smaller particles generally enhancing thermal conductivity due to their higher surface area-to-volume ratio. Smaller nanoparticles tend to increase the viscosity of the nanofluid, affecting the flow dynamics in

the conical gap and potentially leading to higher shear stress and altered velocity profiles. The size of the nanoparticles influences the overall heat transfer efficiency in the conical gap, with optimal particle sizes providing a balance between improved thermal properties and manageable fluid viscosity. The enhanced thermal conductivity and heat transfer efficiency provided by hybrid nanofluids with optimally sized Cu and Al_2O_3 nanoparticles can significantly improve the performance of heat exchangers, leading to more efficient cooling and heating processes in industrial applications.

The focus of this work is the study the three-dimensional flow of a hybrid nanofluid, $Cu + Al_2O_3/H_2O$. While earlier studies [40,41] mostly focused on viscous fluids and nanofluids like carbon nanotubes, we have used the same technique applied in [42], although with a different hybrid nanofluid. This will apply to the assumption that the magnetic field is applied perpendicular to the flow pattern. Additionally, in four distinct scenarios—a stationary disk and a rotating cone, a revolving disk and a stationary cone, a counter-rotating disk and a cone, and a co-rotating disk and a cone—we thoroughly examine and describe the interaction between a disk and a cone [42]. The investigation of temperature and velocity profiles is included in this analysis. We use similarity transformations to translate the mathematical model represented in terms of partial differential equations (PDEs) into ordinary differential equations (ODEs) to make the analysis easier. We next employ the BVP4C technique to produce a dataset for the suggested LM-NN under a range of TRHNF-DC circumstances by altering the magnetic parameters and nanoparticle composition. Ultimately, the intelligent solver LM-NN is trained, tested, and validated to find TRHNF-DC solutions under various conditions. Regression analysis, histograms, absolute error analysis, and comparison with standard solutions allow us to verify the accuracy of the LM-NN scheme in solving the TRHNF-DC model.

Thus, the novelty of the paper lies in the following. This paper presents a novel application in fluid mechanics research by modeling and predicting the complex flow dynamics of hybrid nanofluids in the conical gap between a rotating disk and cone surface using an artificial neural network (ANN). Additionally, the study looks into the improved thermal and flow characteristics of hybrid nanofluids and offers fresh perspectives on how they behave in a rotating system—a domain that has not previously been thoroughly studied. Furthermore, in the analysis of hybrid nanofluid flows, the combination of modern computational approaches (ANN) and experimental fluid dynamics offers a novel viewpoint and perhaps more accurate predictions.

2. Mathematical Modeling

As precised above, the aim in this study is to investigate a situation featuring a cone and a disk holding a non-compressible hybrid nanoliquid subjected to a magnetic field. It is assumed that the cone and disk are either moving or stationary, with their rotational velocity specified in cylindrical coordinates (r, ϕ, z). The symbols Ω and ω represent the rotational speeds of the cone and disk, respectively. B_0 signifies the strength of the magnetic field applied along the z-axis, while any induced magnetic field is ignored. Figure 1 illustrates the geometry of the studied apparatus.

The modeling of heat transfer includes the consideration of viscous dissipation, which is effectively incorporated on the surface of the disk. The surface temperature varies radially and is represented as $T_w = cr^n + T_\infty$, where c and n are constants, and T_∞ is the temperature of the conical surface [40]. Within the conical region, the pressure of the fluid, denoted as p, depends on both the axial distance and the radial distance, r and z. The fundamental equations based on these assumptions are expressed as follows [40–42]:

$$\frac{u}{r} + \frac{\partial w}{\partial z} + \frac{\partial u}{\partial r} = 0, \tag{1}$$

$$\left[w\frac{\partial u}{\partial z} - \frac{v^2}{r} + u\frac{\partial u}{\partial r}\right]\rho_{hnf} = \left[\frac{\partial^2 u}{\partial r^2} + \frac{1}{r}\frac{\partial u}{\partial r} + \frac{\partial^2 u}{\partial z^2} - \frac{u}{r^2}\right]\mu_{hnf} - \frac{\partial p}{\partial r} - B_0^2 u\sigma_{hnf}, \tag{2}$$

$$\left[u\frac{\partial v}{\partial r}+\frac{uv}{r}+w\frac{\partial v}{\partial z}\right]\rho_{hnf}=\left[\frac{\partial^2 v}{\partial z^2}+\frac{1}{r}\frac{\partial v}{\partial r}+\frac{\partial^2 v}{\partial r^2}-\frac{v}{r^2}\right]\mu_{hnf}-B_0^2 v\sigma_{hnf}, \tag{3}$$

$$\left[w\frac{\partial w}{\partial z}+u\frac{\partial w}{\partial r}\right]\rho_{hnf}=\left[\frac{\partial^2 w}{\partial r^2}+\frac{\partial^2 w}{\partial z^2}+\frac{1}{r}\frac{\partial w}{\partial r}\right]\mu_{hnf}-\frac{\partial p}{\partial z}, \tag{4}$$

$$\left[w\frac{\partial T}{\partial z}+u\frac{\partial T}{\partial r}\right](\rho C_p)_{hnf}=B_0^2(v^2+u^2)\sigma_{hnf}+\frac{\partial^2 T}{\partial z^2}k_{hnf}, \tag{5}$$

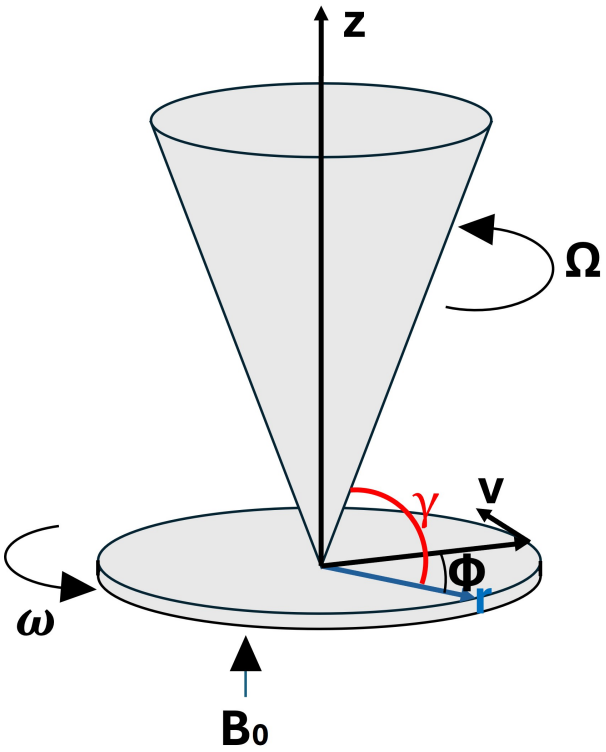

Figure 1. Rotating disk and cone.

In the given equations, (u, v, w) denote the velocity components in the (r, ϕ, z) directions, while B_0 stands for the magnetic field intensity. Moreover, k_{hnf}, v_{hnf}, ρ_{hnf}, σ_{hnf}, and $(\rho C_p)_{hnf}$ signify the thermal conductivity, viscosity, density, electrical conductivity, and heat capacity of the hybrid nanoliquid, respectively.
The mandatory constraints are as follows:

$$\begin{aligned} u=0,\ T=T_w,\ v=r\omega,\ w=0 \quad \text{at}\ z=0 \\ u=0,\ T=T_\infty,\ v=\Omega r,\ w=0 \quad \text{at}\ z=rtan\gamma \end{aligned} \tag{6}$$

Here, γ represents the angular separation between the disk and cone.
To nondimensionalize, we utilize the following similarity transformation [40]:

$$\begin{aligned} u=\frac{F(\zeta)v_f}{r}=U_w F(\zeta),\ v=\frac{G(\zeta)v_f}{r}=U_w G(\zeta),\ u=\frac{H(\zeta)v_f}{r}=U_w H(\zeta), \\ p=\frac{v_f^2\rho P}{r^2}U_w^2 P\rho,\ \zeta=\frac{z}{r},\ M=\frac{B_0^2 v_f\sigma_f}{u_w^2\rho_f},\ \theta=\frac{T-T_\infty}{T_w-T_\infty},\ Pr=\frac{C_p\mu_f}{k_f}. \end{aligned} \tag{7}$$

U_w denotes the surface velocity, Pr stands for the Prandtl number, and M represents the magnetic field. Applying these transformations as described in Equation (7), formulated

Equations (2)–(5) and their respective boundary conditions undergo the following modifications:

$$\zeta F' - H' = 0 \tag{8}$$

$$(1+\zeta^2)F'' + 3\zeta F' + (1-\phi_{Al_2O_3})^{2.5}(1-\phi_{Cu})^{2.5} \times \left[(1-\phi_{Cu})\left(1-\left(1-\frac{\rho_{Al_2O_3}}{\rho f}\right)\phi_{Al_2O_3}\right) + \phi_{Cu}\left(\frac{\rho_{Cu}}{\rho_f}\right)\right]\left[\zeta FF' - HF' + F^2 - G^2\right] + (1-\phi_{Al_2O_3})^{2.5}(1-\phi_{Cu})^{2.5}\left[\zeta p' + 2p - MF\right] = 0 \tag{9}$$

$$(1+\zeta^2)G'' + 3\zeta G' - (1-\phi_{Al_2O_3})^{2.5}(1-\phi_{Cu})^{2.5} \times \left[(1-\phi_{Cu})\left(1-\left(1-\frac{\rho_{Al_2O_3}}{\rho f}\right)\phi_{Al_2O_3}\right) + \phi_{Cu}\left(\frac{\rho_{Cu}}{\rho_f}\right)\right]\left[\zeta FG' - HG'\right] - (1-\phi_{Cu})^{2.5}(1-\phi_{Al_2O_3})^{2.5}MG = 0 \tag{10}$$

$$(1+\zeta^2)H'' + 3\zeta H' + (1-\phi_{Al_2O_3})^{2.5}(1-\phi_{Cu})^{2.5} \times \left[(1-\phi_{Cu})\left(1-\left(1-\frac{\rho_{Al_2O_3}}{\rho f}\right)\phi_{Al_2O_3}\right) + \phi_{Cu}\left(\frac{\rho_{Cu}}{\rho_f}\right)\right]\left[\zeta FH' - HH' + H + FH\right] - (1-\phi_{Cu})^{2.5}(1-\phi_{Al_2O_3})^{2.5}p' = 0, \tag{11}$$

$$\frac{k_{hnf}}{k_{nf}}\left[(1+\zeta^2)\theta'' + \zeta(1-2n)\theta' + n^2\theta\right] + Pr\left[(1-\phi_{Cu})\left(1-\left(1-\frac{(\rho C_p)_{Al_2O_3}}{(\rho C_p)f}\right)\phi_{Al_2O_3}\right) + \phi_{Cu}\left(\frac{(\rho C_p)_{Cu}}{\rho C_{p_f}}\right)\right]\left[\zeta F\theta' - nF\theta - H\theta'\right] + \frac{M}{(1-\phi_{Cu})^{2.5}}(1-\phi_{Al_2O_3})^{2.5}\left[f^2 + G^2\right] = 0 \tag{12}$$

The altered terms are as follows:

$$\begin{aligned} H(0) = F(0) = 0, G(0) = re_w, \theta(0) = 1, \\ F(\zeta_0) = H(\zeta_0) = 0, G(\zeta_0) = Re_\Omega, \theta(\zeta_0) = 0. \end{aligned} \tag{13}$$

The volumetric proportions of Al_2O_3 and Cu are represented by $\phi_{Al_2O_3}$ and ϕ_{Cu}, respectively. Meanwhile, k_{hnf} and k_f denote the thermal conductivity of the hybrid nanoliquid and water, respectively.

The unique thermal properties of the hybrid nanoliquid and water are delineated as follows [43]:

$$v_{hnf} = \frac{\mu_{hnf}}{\rho_{hnf}}, \mu_{hnf} = \frac{\mu_f}{(1-\phi_{Al_2O_3})^{2.5}(1-\phi_{Cu})^{2.5}} \tag{14}$$

$$\frac{\rho_{hnf}}{\rho_f} = (1-\phi_{Cu})\left(1-\left(1-\frac{\rho_{Al_2O_3}}{\rho f}\right)\phi_{Al_2O_3}\right) + \phi_{Cu}\left(\frac{\rho_{Cu}}{\rho_f}\right), \tag{15}$$

$$\frac{(\rho C_p)_{hnf}}{(\rho C_p)_f} = (1-\phi_{Cu})\left(1-\left(1-\frac{(\rho C_p)_{Al_2O_3}}{(\rho C_p)f}\right)\phi_{Al_2O_3}\right) + \phi_{Cu}\left(\frac{(\rho C_p)_{Cu}}{(\rho C_p)_f}\right) \tag{16}$$

$$\frac{\sigma_{hnf}}{\sigma_{bf}} = \left[\frac{(\sigma_{Cu}-\sigma_{bf})3\phi_{Cu}}{(\sigma_{Cu}+2\sigma_{bf}) + (\sigma_{bf}-\sigma_{Cu})\phi_{Cu}} + 1\right], \frac{\sigma_{bf}}{\sigma_f} = \left[\frac{(\sigma_f-\sigma_{Al_2O_3})3\phi_{Al_2O_3}}{(\sigma_{Al_2O_3}-\sigma_f) - (\sigma_{Al_2O_3}+2\sigma_f)\phi_{Cu}} + 1\right], \tag{17}$$

$$k_{hnf} = \left(\frac{2k_{nf} + k_{Cu} + 2\phi_{Cu}(k_{Cu}-k_{nf})}{2k_{nf} + k_{Cu} - \phi_{Cu}(k_{Cu}-k_{nf})}\right)k_{nf}, \frac{k_{nf}}{k_f} = \frac{k_{Al_2O_3} + 2k_f - 2\phi_{Al_2O_3}(k_f - k_{Al_2O_3})}{2k_f + k_{Al_2O_3} + \phi_{Al_2O_3}(k_f - k_{Al_2O_3})}. \tag{18}$$

3. Solution Methodology

To derive ordinary differential equations, partial differential equations undergo a transformation. Employing a similarity transformation tailored for controlling the thermal

aspects of hybrid nanofluid flow in the conical space between a disk and a cone (referred to as TRHNF-DC), the reference dataset is utilized in Matlab via the BVP4C solution method. TRHNF-DC, implemented in Matlab, utilizes a dataset with the Levenberg–Marquardt method and a backpropagated artificial neural network (ANN). A strategic approach is adopted with an intelligent Levenberg–Marquardt neural network, allocating 80% of the data for training, 10% for validation, and 10% for testing. This article explores three scenarios involving various instances of TRHNF-DC.

3.1. Bvp4c Method And Usage on Cone–Disk Apparatus

BVP4C, or Boundary Value Problem solver for Ordinary Differential Equations, is a numerical method used to solve boundary value problems efficiently. It works by discretizing the problem domain and approximating the solution iteratively until convergence is achieved. When applied to cone and disk apparatus, the BVP4C method assists in modeling the flow of fluids or heat transfer within the apparatus. By defining appropriate boundary conditions, it accurately predicts the behavior of the system, aiding in design and optimization processes. In conjunction with neural networks, the BVP4C method can enhance its predictive capabilities by incorporating learned patterns and relationships from data. Neural networks can assist in approximating complex boundary conditions or optimizing parameters for improved accuracy. The integration of BVP4C with neural networks allows for a more robust and adaptive approach to solving problems related to cone and disk apparatus, enabling better understanding and control of the underlying processes.

3.2. Artificial Neural Network

The neural network diagram of TRHNF-DC is depicted in Figure 2. The usage of a neural network in the approach is motivated by the following.

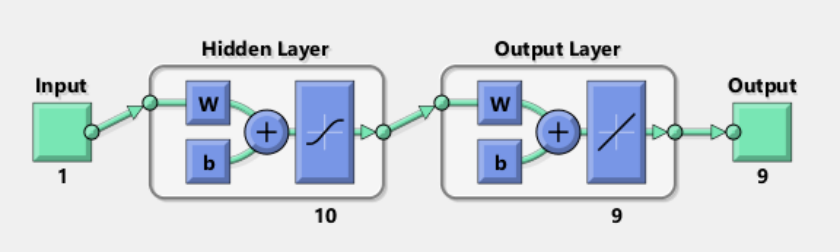

Figure 2. Neural network diagram for TRHNF-DC.

BVP4C is a robust numerical method specifically designed for solving boundary value problems, and it can provide accurate solutions efficiently for many types of problems. If a neural network is trained on data generated using BVP4C, it might not necessarily be more efficient, but it learns to efficiently capture flow dynamics, enhancing solution speed and adaptability. Also, there could be scenarios where using a neural network offers advantages such as generalization to unseen data or the ability to handle noisy or incomplete input. Additionally, once trained, a neural network can provide solutions very quickly, making it preferable for certain real-time or iterative applications. This fusion leverages the strengths of both numerical methods and neural networks to tackle complex flow dynamics problems effectively. In the conducted experiments, the ANN inputs are the parameters involved in the model and the outputs come after solving the model. The ANN has one hidden layer of 10 cells and the output layer has 9 cells.

3.3. Training and Testing Database

The generated database comprises a comprehensive set of samples to cover various scenarios encountered in the cone and disk apparatus. It includes data from experiments or simulations representing different configurations such as stationary disk and rotating cone, stationary cone and rotating disk, and combinations thereof. The database encompasses

a significant number of samples to ensure thorough coverage of the parameter space. Data are generated each time by varying 1 parameter and keeping other parameters fixed. Inputs to the database typically include variables such as fluid properties, geometrical dimensions of the apparatus, rotational speeds, and operating conditions. Outputs from the database consist of observed or simulated behaviors of interest, such as velocity profiles and temperature profiles. These outputs are essential for training the neural network to predict system responses accurately. By encompassing diverse configurations and parameter ranges, the database ensures that the trained neural network can effectively generalize to unseen cases and accurately predict outcomes for various operating conditions encountered in practical applications of the cone and disk apparatus. The Levenberg–Marquardt (LM) algorithm is a popular optimization method used for training neural networks, particularly because of its efficiency and speed in converging to a solution. When allocating data for training, validation, and testing in the context of the LM neural network, the rationale involves several key considerations. The data are typically split into three sets: training, validation, and testing. The training set is used to adjust the weights and biases of the network, the validation set is used to tune hyperparameters and prevent overfitting, and the testing set is used to evaluate the final model's performance. This allocation ensures that the model is both trained well and generalizable. The LM algorithm is powerful and can easily overfit the training data. By setting aside a validation set, the model's performance on unseen data can be monitored during training. If the validation error starts to increase while the training error decreases, it indicates overfitting, and training can be stopped early (early stopping). The test set, which is not used during training or validation, provides an unbiased evaluation of the final model's performance. This ensures that the model's accuracy and generalization capabilities are accurately assessed. The validation set is crucial for fine-tuning the hyperparameters (such as learning rate, network architecture, and regularization parameters). The LM algorithm benefits from this as it helps in finding the optimal balance between underfitting and overfitting. During the training process, the LM algorithm can use the validation set to monitor the network's performance at each iteration. This helps in deciding when to stop training to avoid overfitting, known as early stopping. The allocation of a validation set is particularly important for this purpose.

The values of parameters are $M = 0, 2, 4$, $\phi_{Al_2O_3} = 0.02$, $\phi_{Cu} = 0.02$, $Re_\omega = 0.3$, $Re_\Omega = 0.13$, $\eta = 2$, $n = 1$, and $Pr = 6.2$ and the relevant properties of alumina, copper and water are shown in Table 1.

Table 1. The thermal properties of alumina, copper, and water [43–47].

Property	H_2O	Cu	Al_2O_3
Thermal Conductivity (W/mK)	0.6071	400	40
Density (kg/m^3)	997	8933	3970
Specific Heat (J/kgK)	4180	385	765
Electrical Conductivity (s/m)	5.5×10^{-6}	59.6×10^6	35×10^6

4. Results and Discussion

This section presents different results obtained from applying the proposed approach on the established model. Different performance metrics values are reported along with illustrations that show the effectiveness of the system.

4.1. Ann Performance Measures

Table 2 presents the numerical outcomes related to the training, testing, and validation phases, along with performance metrics, total epochs, and parameters governing backpropagation, including the magnetic number (M) (Scenario 1). These results illuminate their influence on the axial velocity profile, $F(\zeta)$, within the framework of TRHNF-DC. Meanwhile, Table 2 also illustrates the fluctuations of cone velocity, Re_Ω, and angular velocity,

Re_ω, on the radial profile, $G(\zeta)$ (Scenario 2). Similarly, it demonstrates the variations of the magnetic number (M) on the temperature profile, $\theta(\zeta)$ (Scenario 3).

Table 2. Metrics from the neural network training and testing for the three considered scenarios.

Case	MSE			Performance	Grad	Mu	Epochs
	Training	Validation	Testing				
Scenario 1, Influence of M on $F(\zeta)$							
1	2.0183×10^{-10}	3.2274×10^{-10}	2.9818×10^{-10}	2.02×10^{-10}	9.76×10^{8}	1.00×10^{9}	98
2	1.7456×10^{-10}	1.5390×10^{-17}	3.2871×10^{-10}	1.75×10^{-10}	9.96×10^{8}	1.00×10^{9}	104
3	4.1089×10^{-10}	4.7110×10^{-10}	6.1340×10^{-10}	4.11×10^{-10}	9.88×10^{8}	1.00×10^{9}	82
4	1.9404×10^{-10}	2.6040×10^{-10}	4.3901×10^{8}	1.94×10^{-10}	9.98×10^{8}	1.00×10^{9}	109
5	1.9895×10^{-10}	1.4231×10^{-10}	1.2395×10^{8}	1.99×10^{-10}	9.75×10^{8}	1.00×10^{9}	95
6	3.3441×10^{-10}	7.5751×10^{-10}	1.8547×10^{7}	3.34×10^{-10}	9.90×10^{8}	1.00×10^{9}	77
Scenario 2, Influence of Re_Ω and Re_ω on radial profile $G(\zeta)$							
1	8.1394×10^{-10}	1.3232×10^{9}	8.0754×10^{-10}	8.14×10^{-10}	9.95×10^{8}	1.00×10^{8}	299
2	1.5467×10^{-10}	8.1606×10^{-10}	3.1606×10^{-10}	1.55×10^{-10}	9.83×10^{8}	1.00×10^{9}	113
3	1.9272×10^{-13}	3.5877×10^{-11}	3.0439×10^{-13}	1.93×10^{-13}	9.95×10^{8}	1.00×10^{11}	229
4	2.4139×10^{-10}	7.7476×10^{-10}	2.4731×10^{-10}	2.41×10^{-10}	1.00×10^{7}	1.00×10^{8}	389
5	1.2517×10^{-10}	1.7883×10^{-10}	2.1113×10^{-10}	1.25×10^{-10}	9.87×10^{8}	1.00×10^{9}	135
6	2.2453×10^{-10}	2.7066×10^{-10}	2.7337×10^{-10}	2.25×10^{-10}	9.99×10^{8}	1.00×10^{8}	499
Scenario 3, Influence of M on $\theta(\zeta)$							
1	1.0431×10^{-10}	1.7383×10^{-10}	1.5413×10^{-10}	1.04×10^{-10}	9.99×10^{8}	1.00×10^{9}	119
2	1.5565×10^{-11}	3.0643×10^{-11}	1.0060×10^{9}	1.56×10^{-11}	9.93×10^{8}	1.00×10^{10}	75
3	9.4899×10^{-12}	4.7135×10^{-11}	1.1648×10^{-11}	9.49×10^{-12}	9.91×10^{8}	1.00×10^{10}	101
4	1.7713×10^{-11}	9.5478×10^{-11}	3.6367×10^{-11}	1.77×10^{-11}	9.88×10^{8}	1.00×10^{10}	75
5	3.0153×10^{-10}	4.1094×10^{-10}	2.6628×10^{-10}	3.02×10^{-10}	9.85×10^{8}	1.00×10^{9}	86
6	2.2186×10^{-10}	2.6282×10^{-10}	3.9525×10^{-10}	2.22×10^{-10}	9.95×10^{8}	1.00×10^{9}	109

Table 2 shows the following measures:

- MSE (Mean Squared Error) in neural networks quantifies the average squared difference between predicted and actual values. It serves as a key metric for assessing the model's performance in regression tasks. Lower MSE values indicate better accuracy and closer alignment between predictions and true outcomes.
- "Performance" refers to the overall effectiveness of the model in achieving its intended task, whether it is classification, regression, or another objective. Performance metrics such as accuracy, precision, recall, F1-score, and others provide quantitative measures of how well the model performs on a given dataset. Evaluating performance is crucial for assessing the model's reliability and suitability for practical applications.
- The gradient represents the rate of change of the loss function with respect to the model's parameters. It guides the optimization process, indicating the direction and magnitude of adjustments required to minimize the loss and improve the model's performance during training.
- Mu often represents the learning rate, determining the size of the steps taken during optimization. Adjusting mu impacts the convergence speed and stability of the training process, influencing the network's ability to learn effectively.

- Epoch refers to a single pass of the entire training dataset through the model. Multiple epochs are typically required to iteratively adjust the model's parameters to minimize the loss function and improve performance. Increasing the number of epochs allows the model to learn more complex patterns in the data.

Figure 3 depicts the variation in Mean Squared Error (MSE) and the regression analysis for Scenario 1: case 1. It is observed that the optimal training efficiency is 3.2275×10^{-10} at epoch 98, with a gradient of 9.75×10^{-9} and a learning rate (μ) of 1×10^{-9} at epoch 98. Regression plots assess the relationship between output and desired output; if R is close to 1, the interaction is close; if R is close to 0, a stochastic relationship is implied. The lower the MSE value, the more dependable the solution. A side-by-side evaluation of the ANN results with the reference solution is shown in Figure 2b, indicating a high degree of agreement between the two solutions, with MSE errors in the order of 1×10^{-10}, showcasing the viability of the suggested method.

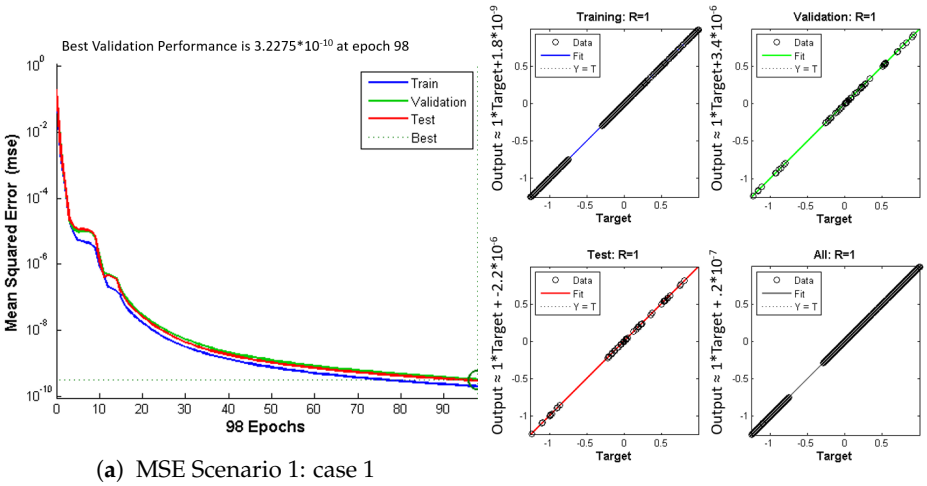

(**a**) MSE Scenario 1: case 1

(**b**) Regression analysis Scenario 1: case 1

Figure 3. Plots for solving M for $f^{'}(\zeta)$.

Figure 4 illustrates the fluctuation in MSE and the regression analysis for Scenario 2: case 6, and for Scenario 3: case 6. From Figure 4a,b, it can be seen that the best training results are $[2.7067 \times 10^{-10}, 2.6283 \times 10^{-10}]$ at epochs [499,109] for solving Re_{ω} and Re_{Ω} for $G(\zeta)$, and M for $\theta(\zeta)$, respectively. These charts illustrate the effective validation of the training data across various scenarios. The regression graphs are shown in Figure 4c,d.

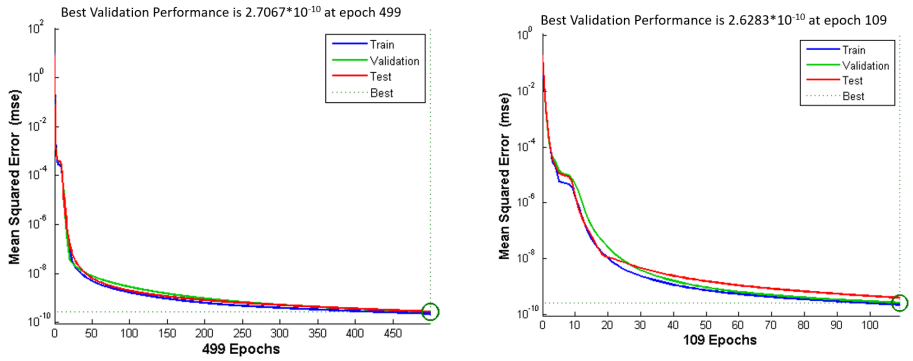

(**a**) MSE Scenario 2: case 1

(**b**) MSE Scenario 3: case 1

Figure 4. *Cont.*

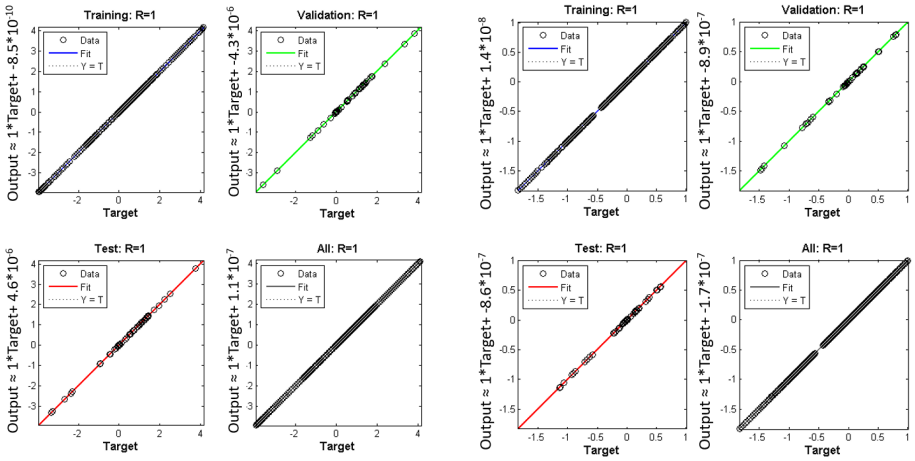

(**c**) Regression Analysis Scenario 2: case 1 (**d**) Regression Analysis Scenario 3: case 1

Figure 4. (**a**,**c**): Plots of Re_ω and Re_Ω for $G(\zeta)$. (**b**,**d**): Plots for solving M for $\theta(\zeta)$.

4.2. Physical Parameters

This section delves into the investigation of various physical parameters concerning temperature and velocity distributions within a system comprising a rotating disk and cone, a setup critical to the overall inquiry.

Figure 5 examines in its upper left part the influence of the magnetic number (M) on the axial velocity profile $(F(\zeta))$. A rise in M leads to a decrease in fluid velocity for both copper (Cu) and aluminum oxide (Al_2O_3) hybrid nanoliquids due to the Lorentz force impeding fluid velocity. In its upper right and lower left parts, Figure 5 depicts the effect of volume fraction factors, specifically $\phi_{Al_2O_3}$ and ϕ_{Cu}, on the axial velocity profile. An increase in volume fraction parameters enhances the boundary layer thickness, resulting in a decline in the velocity profile. Finally, in its lower right part, the figure explores the impact of the magnetic parameter (M) on the radial velocity profile, $G(\zeta)$, showing similar behavior to the axial velocity discussed earlier.

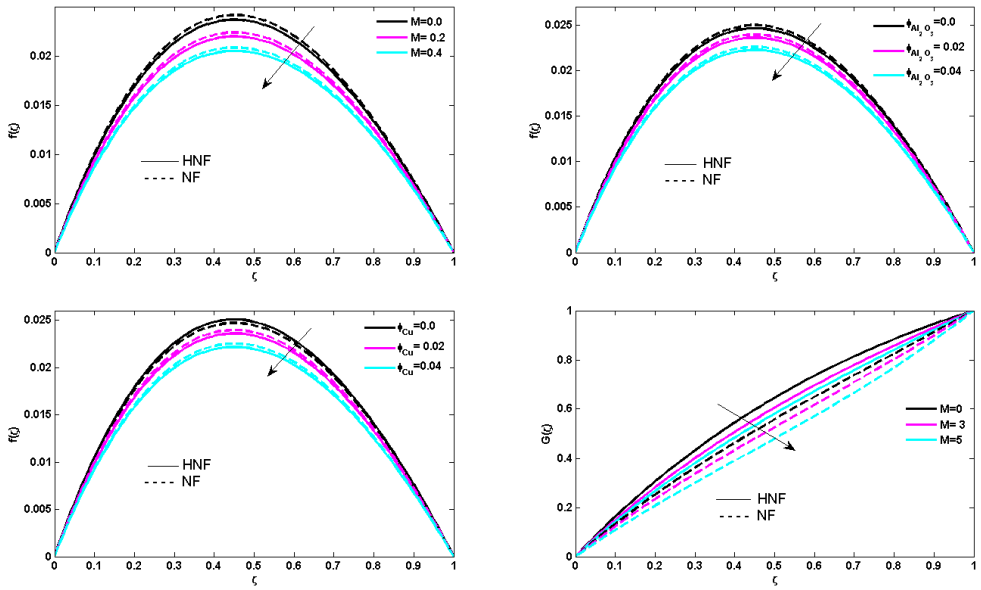

Figure 5. (**Up-left**): Impact of M on $F(\zeta)$. (**Up-right:**) Impact of $\phi_{Al_2O_3}$ on $F(\zeta)$. (**Down-left**): Impact of ϕ_{Cu} on $F(\zeta)$. (**Down-right**): Influence of M on $G(\zeta)$.

Figure 6 investigates first the influence of volume fraction factors of iron oxide on the radial velocity profile, with changes in $\phi_{Al_2O_3}$ exhibiting analogous behavior to the axial velocity. Then, the figure examines the influence of the copper volume fraction parameter (ϕ_{Cu}) on the radial velocity profile, $G(\zeta)$, indicating similar variations as observed in the axial velocity. A brief discussion of four instances of disk and cone angular motion is later presented in Figure 6. Case (1) describes the scenario where the cone is spinning and the disk is at rest, leading to the highest flow intensity near the cone's vicinity, influencing the radial profile, $G(\zeta)$, positively through the cone's angular velocity variation, Re_Ω. Case (2) shows the opposite trend, with the disk moving while the cone is stationary, resulting in resistance at the cone wall due to the no-slip condition. Scenario (3) demonstrates the dominance of the flow field over Re_Ω and Re_ω, respectively, as there is minimal resistance to both cone and disk rotating in the same direction. In contrast, the figure finally illustrates the reduction in fluid velocity due to the counter-rotation of the disk and cone, leading to the highest resistance, as demonstrated by Case (4).

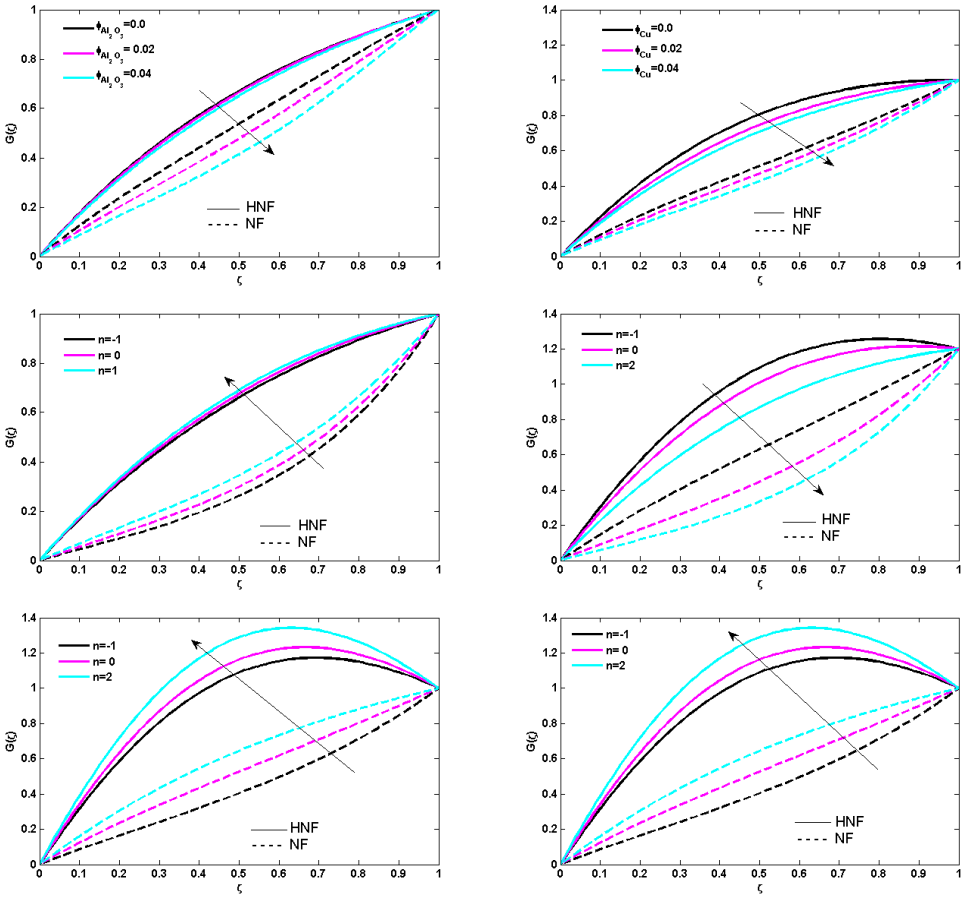

Figure 6. (**Up-left**): Influence of M on $G(\zeta)$. (**Up-right**): Influence of $\phi_{Al_2O_3}$ on $G(\zeta)$. (**Middle-left**): Case (1) influence over $G(\zeta)$. (**Middle-right**): Case (2) influence over $G(\zeta)$. (**Down-left**): Case (3) influence on $G(\zeta)$. (**Down-right**): Case (3) influence on $G(\zeta)$.

Figure 7 first describes the type of temperature distribution, $\theta(\zeta)$, vs magnetic strength, M, where the Lorentz force impedes fluid motion, gradually raising the fluid temperature, $\theta(\zeta)$. The addition of $\phi_{Al_2O_3}$ and ϕ_{Cu} nanoparticles to the carrier fluid increases its viscosity and heat absorption capacity, as evidenced later in Figure 7. The figure then showcases the dominance of the Prandtl number, Pr, over temperature distribution, where fluids with high Prandtl numbers exhibit lower thermal diffusivity, and vice versa.

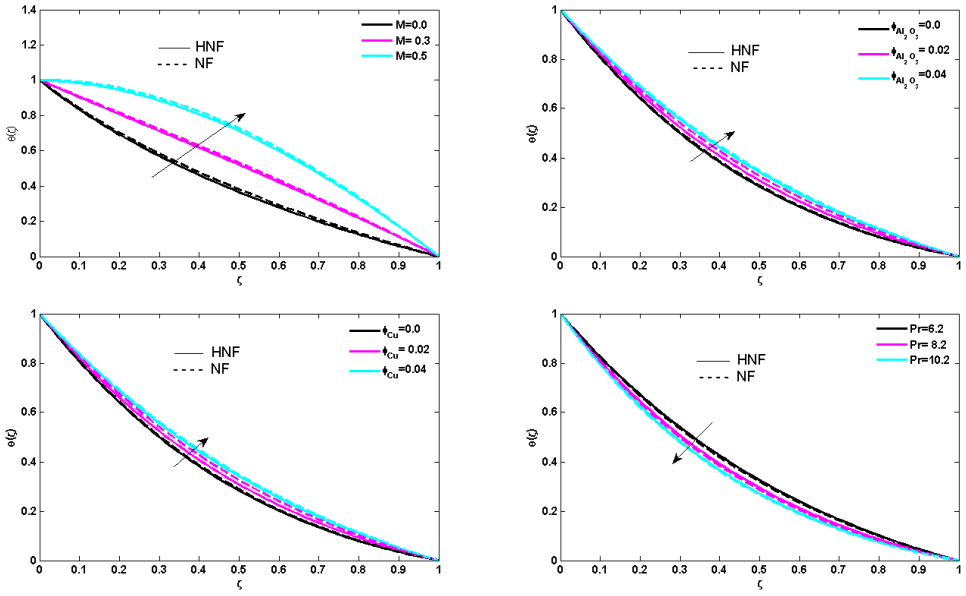

Figure 7. (**Up-left**): Influence of M on $\theta(\zeta)$. (**Up-right**): Influence of $\phi_{Al_2O_3}$ on $\theta(\zeta)$. (**Down-left**): Influence of ϕ_{Cu} on $\theta(\zeta)$. (**Down-right**): Influence of Pr on $\theta(\zeta)$.

5. Conclusions

In this current investigation, practical implementations are reexamined, primarily focusing on the disk–cone device utilized in industrial settings. We examine a unique blend of hybrid nanofluid containing copper (Cu) and (Al_2O_3) nanoparticles, which can be either in motion or stationary. In both scenarios, they can rotate in either a counter- or co-directional manner under the influence of a magnetic field. The effects of various physical parameters on velocity and temperature are elucidated through graphical representations. The key discoveries reached are as follows:

- The rate of heat transfer and the velocity of the carrier fluid are boosted by increasing amounts of solid nanoparticles.
- Conversely, when it comes to the magnetic parameter, M, an opposite trend is noticed. An increase in M leads to a decrease in fluid velocity and an increase in temperature, θ, due to the Lorentz force effect, which acts as a retarding force.
- The radial velocity profile, G, is positively impacted by the local Reynolds numbers, Re_ω and Re_Ω, which are based on the angular velocity of the disk and cone, respectively.
- The conclusion drawn is that the momentum boundary layer improves when the cone and disk spin in the same direction, whereas a decrease in the momentum boundary layer is observed when they rotate in opposite directions.
- It is evident that the temperature experiences a slight increase across the thermal layer under normal tip angles. However, there is minimal impact observed for minor gap angles due to the emergence of a critical power index $n = -1, 0, 2$. Consequently, heat transfer from the disk surface ceases, rendering the fluid at the disk surface to act as an insulator, as there is no heat transfer occurring.
- This study employs an artificial neural network (ANN) approach to model and predict the complex flow dynamics of hybrid nanofluids in the conical gap between a rotating disk and cone surface, a novel application in fluid mechanics research.
- The research investigates the enhanced thermal and flow properties of hybrid nanofluids, providing new insights into their behavior in a rotating system, which has not been extensively explored before.

- The combination of advanced computational techniques (ANN) with experimental fluid dynamics offers a unique perspective and potentially more accurate predictions in the analysis of hybrid nanofluid flows.

Author Contributions: Conceptualization, R.G., Z.A.B. and J.M.H.B.; methodology, Z.A.B. and J.M.H.B.; software, Z.A.B. and J.M.H.B.; validation, Z.A.B. and J.M.H.B.; formal analysis, R.G., Z.A.B. and J.M.H.B.; investigation, R.G., Z.A.B. and J.M.H.B.; resources, Z.A.B. and J.M.H.B.; writing—original draft preparation, Z.A.B. and J.M.H.B.; writing—review and editing, R.G. and Z.A.B.; supervision R.G. All authors have read and agreed to the published version of the manuscript.

Funding: This research received no external funding.

Data Availability Statement: The original contributions presented in the study are included in the article. Further inquiries can be directed to the corresponding author.

Conflicts of Interest: The authors declare no conflict of interest.

References

1. Ma, Y.; Mohebbi, R.; Rashidi, M.M.; Yang, Z. Study of nanofluid forced convection heat transfer in a bent channel by means of lattice Boltzmann method. *Phys. Fluids* **2018**, *30*, 032001. [CrossRef]
2. Phan-Thien, N. Cone-and-plate flow of the Oldroyd-B fluid is unstable. *J.-Non-Newton. Fluid Mech.* **1985**, *17*, 37–44. [CrossRef]
3. Spruell, C.; Baker, A.B. Analysis of a high-throughput cone-and-plate apparatus for the application of defined spatiotemporal flow to cultured cells. *Biotechnol. Bioeng.* **2013**, *110*, 1782–1793. [CrossRef] [PubMed]
4. Owen, J.M. Flow and Heat Transfer in Rotating-Disc Systems. In Proceedings of the 1992 International Symposium on Heat Transfer in Turbomachinery, Marathon, Greece, 24–28 August 1992; Begellhouse: Danbury, CT, USA, 1994. [CrossRef]
5. Choi, U.S. Enhancing Thermal Conductivity of Fluids with Nanoparticles, Developments and Application of Non-Newtonian Flows. *Asme J. Heat Transf.* **1995**, *66*, 99–105.
6. Turkyilmazoglu, M. On the purely analytic computation of laminar boundary layer flow over a rotating cone. *Int. J. Eng. Sci.* **2009**, *47*, 875–882. [CrossRef]
7. Garrett, S.J.; Hussain, Z.; Stephen, S.O. Boundary-Layer Transition on Broad Cones rotating in an Imposed Axial Flow. *AIAA J.* **2010**, *48*, 1184–1194. [CrossRef]
8. Towers, P.; Garrett, S. Similarity solutions of compressible flow over a rotating cone with surface suction. *Therm. Sci.* **2016**, *20*, 517–528. [CrossRef]
9. Rasool, G.; Zhang, T. Darcy-Forchheimer nanofluidic flow manifested with Cattaneo-Christov theory of heat and mass flux over non-linearly stretching surface. *PLoS ONE* **2019**, *14*, e0221302. [CrossRef]
10. Shirejini, S.Z.; Rashidi, S.; Esfahani, J. Recovery of drop in heat transfer rate for a rotating system by nanofluids. *J. Mol. Liq.* **2016**, *220*, 961–969. [CrossRef]
11. Turkyilmazoglu, M. Effects of uniform radial electric field on the MHD heat and fluid flow due to a rotating disk. *Int. J. Eng. Sci.* **2012**, *51*, 233–240. [CrossRef]
12. Kumar, R.; Seth, G.S.; Bhattacharyya, A. Entropy generation of von Karman's radiative flow with Al2O3 and Cu nanoparticles between two coaxial rotating disks: A finite-element analysis. *Eur. Phys. J. Plus* **2019**, *134*, 597. [CrossRef]
13. Bhattacharyya, A.; Seth, G.S.; Kumar, R.; Chamkha, A.J. Simulation of Cattaneo–Christov heat flux on the flow of single and multi-walled carbon nanotubes between two stretchable coaxial rotating disks. *J. Therm. Anal. Calorim.* **2019**, *139*, 1655–1670. [CrossRef]
14. Nazari, S.; Ellahi, R.; Sarafraz, M.M.; Safaei, M.R.; Asgari, A.; Akbari, O.A. Numerical study on mixed convection of a non-Newtonian nanofluid with porous media in a two lid-driven square cavity. *J. Therm. Anal. Calorim.* **2019**, *140*, 1121–1145. [CrossRef]
15. Ahmed, J.; Khan, M.; Ahmad, L. Effectiveness of homogeneous–heterogeneous reactions in Maxwell fluid flow between two spiraling disks with improved heat conduction features. *J. Therm. Anal. Calorim.* **2019**, *139*, 3185–3195. [CrossRef]
16. Rashidi, M.M.; Ghahremanian, S.; Toghraie, D.; Roy, P. Effect of solid surface structure on the condensation flow of Argon in rough nanochannels with different roughness geometries using molecular dynamics simulation. *Int. Commun. Heat Mass Transf.* **2020**, *117*, 104741. [CrossRef]
17. Siddiqui, A.; Manzoor, N.; Maqbool, K.; Mann, A.; Shaheen, S. Magnetohydrodynamic flow induced by ciliary movement: An application to lower respiratory track diseases. *J. Magn. Magn. Mater.* **2019**, *480*, 164–170. [CrossRef]
18. Hafidzuddin, M.; Nazar, R.; Arifin, N.M. Application of the Keller-box method to magnetohydrodynamic rotating flow over a permeable shrinking surface. *Embrac. Math. Divers.* **2019**, *130*, 36–41.
19. Oyelakin, I.S.; Lalramneihmawii, P.; Mondal, S.; Nandy, S.K.; Sibanda, P. Thermophysical analysis of three-dimensional magnetohydrodynamic flow of a tangent hyperbolic nanofluid. *Eng. Rep.* **2020**, *2*, e12144. [CrossRef]

20. Tlili, I.; Nabwey, H.A.; Ashwinkumar, G.P.; Sandeep, N. 3-D magnetohydrodynamic AA7072-AA7075/methanol hybrid nanofluid flow above an uneven thickness surface with slip effect. *Sci. Rep.* **2020**, *10*, 4265. [CrossRef]
21. Khan, U.; Zaib, A.; Khan, I.; Nisar, K.S. Activation energy on MHD flow of titanium alloy (Ti6Al4V) nanoparticle along with a cross flow and streamwise direction with binary chemical reaction and non-linear radiation: Dual Solutions. *J. Mater. Res. Technol.* **2020**, *9*, 188–199. [CrossRef]
22. Goodarzi, M.; Toghraie, D.; Reiszadeh, M.; Afrand, M. Experimental evaluation of dynamic viscosity of ZnO–MWCNTs/engine oil hybrid nanolubricant based on changes in temperature and concentration. *J. Therm. Anal. Calorim.* **2018**, *136*, 513–525. [CrossRef]
23. Turkyilmazoglu, M. Single phase nanofluids in fluid mechanics and their hydrodynamic linear stability analysis. *Comput. Methods Programs Biomed.* **2020**, *187*, 105171. [CrossRef] [PubMed]
24. Ahmad, I.; Raja, M.A.Z.; Ramos, H.; Bilal, M.; Shoaib, M. Integrated neuro-evolution-based computing solver for dynamics of nonlinear corneal shape model numerically. *Neural Comput. Appl.* **2020**, *33*, 5753–5769. [CrossRef]
25. Ahmad, I.; Raja, M.A.Z.; Bilal, M.; Ashraf, F. Bio-inspired computational heuristics to study Lane–Emden systems arising in astrophysics model. *SpringerPlus* **2016**, *5*, 1866. [CrossRef] [PubMed]
26. Sabir, Z.; Wahab, H.A.; Umar, M.; Sakar, M.G.; Raja, M.A.Z. Novel design of Morlet wavelet neural network for solving second order Lane–Emden equation. *Math. Comput. Simul.* **2020**, *172*, 1–14. [CrossRef]
27. Khan, I.; Raja, M.A.Z.; Shoaib, M.; Kumam, P.; Alrabaiah, H.; Shah, Z.; Islam, S. Design of Neural Network with Levenberg-Marquardt and Bayesian Regularization Backpropagation for Solving Pantograph Delay Differential Equations. *IEEE Access* **2020**, *8*, 137918–137933. [CrossRef]
28. Bukhari, A.H.; Raja, M.A.Z.; Sulaiman, M.; Islam, S.; Shoaib, M.; Kumam, P. Fractional Neuro-Sequential ARFIMA-LSTM for Financial Market Forecasting. *IEEE Access* **2020**, *8*, 71326–71338. [CrossRef]
29. Jadoon, I.; Raja, M.A.Z.; Junaid, M.; Ahmed, A.; ur Rehman, A.; Shoaib, M. Design of evolutionary optimized finite difference based numerical computing for dust density model of nonlinear Van-der Pol Mathieu's oscillatory systems. *Math. Comput. Simul.* **2021**, *181*, 444–470. [CrossRef]
30. Bukhari, A.H.; Sulaiman, M.; Raja, M.A.Z.; Islam, S.; Shoaib, M.; Kumam, P. Design of a hybrid NAR-RBFs neural network for nonlinear dusty plasma system. *Alex. Eng. J.* **2020**, *59*, 3325–3345. [CrossRef]
31. Sabir, Z.; Raja, M.A.Z.; Guirao, J.L.G.; Shoaib, M. Integrated intelligent computing with neuro-swarming solver for multi-singular fourth-order nonlinear Emden–Fowler equation. *Comput. Appl. Math.* **2020**, *39*, 307. [CrossRef]
32. Sabir, Z.; Baleanu, D.; Shoaib, M.; Raja, M.A.Z. Design of stochastic numerical solver for the solution of singular three-point second-order boundary value problems. *Neural Comput. Appl.* **2020**, *33*, 2427–2443. [CrossRef]
33. Ahmad, S.u.I.; Faisal, F.; Shoaib, M.; Raja, M.A.Z. A new heuristic computational solver for nonlinear singular Thomas–Fermi system using evolutionary optimized cubic splines. *Eur. Phys. J. Plus* **2020**, *135*, 55. [CrossRef]
34. Imran, A.; Akhtar, R.; Zhiyu, Z.; Shoaib, M.; Zahoor Raja, M.A. MHD and heat transfer analyses of a fluid flow through scraped surface heat exchanger by analytical solver. *AIP Adv.* **2019**, *9*, 075201. [CrossRef]
35. Waseem, W.; Sulaiman, M.; Islam, S.; Kumam, P.; Nawaz, R.; Raja, M.A.Z.; Farooq, M.; Shoaib, M. A study of changes in temperature profile of porous fin model using cuckoo search algorithm. *Alex. Eng. J.* **2020**, *59*, 11–24. [CrossRef]
36. Umar, M.; Sabir, Z.; Raja, M.A.Z.; Shoaib, M.; Gupta, M.; Sánchez, Y.G. A Stochastic Intelligent Computing with Neuro-Evolution Heuristics for Nonlinear SITR System of Novel COVID-19 Dynamics. *Symmetry* **2020**, *12*, 1628. [CrossRef]
37. Cheema, T.N.; Raja, M.A.Z.; Ahmad, I.; Naz, S.; Ilyas, H.; Shoaib, M. Intelligent computing with Levenberg–Marquardt artificial neural networks for nonlinear system of COVID-19 epidemic model for future generation disease control. *Eur. Phys. J. Plus* **2020**, *135*, 932. [CrossRef] [PubMed]
38. Raja, M.A.Z.; Umar, M.; Sabir, Z.; Khan, J.A.; Baleanu, D. A new stochastic computing paradigm for the dynamics of nonlinear singular heat conduction model of the human head. *Eur. Phys. J. Plus* **2018**, *133*. [CrossRef]
39. Hammal, S.; Bourahla, N.; Laouami, N. Neural-Network Based Prediction of Inelastic Response Spectra. *Civ. Eng. J.* **2020**, *6*, 1124–1135. [CrossRef]
40. Turkyilmazoglu, M. On the fluid flow and heat transfer between a cone and a disk both stationary or rotating. *Math. Comput. Simul.* **2020**, *177*, 329–340. [CrossRef]
41. Gul, T.; Gul, R.S.; Noman, W.; Saeed, A.; Mukhtar, S.; Alghamdi, W.; Alrabaiah, H. CNTs-Nanofluid flow in a Rotating system between the gap of a disk and cone. *Phys. Scr.* **2020**, *95*, 125202. [CrossRef]
42. Gul, T.; Ullah, K.; Bilal, M.; Alghamdi, W.; Asjad, M.; Abdeljawad, T. Hybrid nanofluid flow within the conical gap between the cone and the surface of a rotating disk. *Sci. Rep.* **2021**, *11*, 1180. [CrossRef] [PubMed]
43. Devi, S.S.U.; Devi, S.P.A. Nigerian Mathematical Society Heat Transfer Enhancement of Cu—Al_2O_3 / Water Hybrid Nanofluid Flow Over a Stretching Sheet. *J. Niger. Math. Soc.* **2017**, *36*, 419–433.
44. Zakaria, I.; Azmi, W.; Mohamed, W.; Mamat, R.; Najafi, G. Experimental Investigation of Thermal Conductivity and Electrical Conductivity of Al_2O_3 Nanofluid in Water—Ethylene Glycol Mixture for Proton Exchange Membrane Fuel Cell Application. *Int. Commun. Heat Mass Transf.* **2015**, *61*, 61–68. [CrossRef]
45. Kováčik, J.; Emmer, Š.; Bielek, J. Thermal conductivity of Cu-graphite composites. *Int. J. Therm. Sci.* **2015**, *90*, 298–302. [CrossRef]

46. Krishna, M.V.; Ahammad, N.A.; Chamkha, A.J. Radiative MHD flow of Casson hybrid nanofluid over an infinite exponentially accelerated vertical porous surface. *Case Stud. Therm. Eng.* **2021**, *27*, 101229. [CrossRef]
47. Seonja, S.; Changkook, J.; Kyeongho, S.; Juhyung, K.; Youngseok, K.; Jaeuk, C. Synthesis of Thermal Compound and Its Application as a Thermal Interface Material of Power Module. In Proceedings of the 2018 17th IEEE Intersociety Conference on Thermal and Thermomechanical Phenomena in Electronic Systems (ITherm), San Diego, CA, USA, 29 May–1 June 2018; pp. 482–486. [CrossRef]